Journal of Materials Chemistry A

Accepted Manuscript

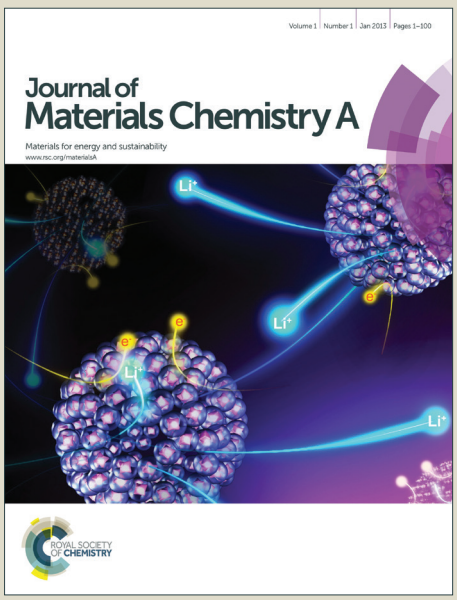

ROYAL SOCIETY OF CHEMISTRY

www.rsc.org/materialsA

Supercritical Fluid Assisted Synthesis of N-doped Graphene Nanosheets and Its Capacitance Behavior in Ionic liquid and Aqueous Electrolyte

Marappan Sathish,*[a,b] Satoshi Mitani,[a] Takkaki Tomai[a] and Itaru Honma*[a]

[a]Institute of Multidisciplinary Research for Advanced Materials, Tohoku University, 2-1-1, Katahira, Sendai 980 8577, Japan.
[b]Functional Materials Division, CSIR-Central Electrochemical Research Institute, Karaikudi - 630 006, India.
E.mail: marappan.sathish@gmail.com; i.honma@tagen.tohoku.ac.jp

Abstract:-

N-doped graphene nanosheets (N-doped GNS) were obtained using single step supercritical fluid assisted reaction of N-containing organic compounds with graphene oxide (GO) solution. N-doped GNS sample shows a capacitance of 280 F/g in aqueous 1M H_2SO_4 (0.8 V) and 104 F/g in ionic liquid EMI-TFSA (3.6V). NE-GNS electrode shows an energy density of 8 Wh/Kg and 40 Wh/Kg in 1M H_2SO_4 and EMI-TFSA, respectively. The nature of chemical bonding and amount of N doping in the graphene samples was estimated using XPS spectroscopy. The amount of N-doping varies with nature of the N-containing organic compounds and the supercapacitance behaviour depends on the amount of N-doping as well as nature of N-doping in the graphene. TEM, FE-SEM images and Raman spectroscopic characterization reveals the presence of few layer N-doped GNS. FT-IR spectra exhibits the presence of various functional groups on N-doped GNS XRD diffraction analysis showed the weakly stacked N-doped GNS due to the N-doping and the presence of N-containing functional groups on N-doped GNS. The cyclic voltammetry studies showed the capacitance behaviour of N-doped GNS electrodes at high potential window of 4.25 V in ionic liquids. The charge-discharge profile showed the stable charge-discharge behaviour of the N-doped GNS electrodes.

Keywords:- N-doping, graphene, supercapacitors, ionic liquids, energy storage

Introduction

Supercritical fluid assisted material synthesis has emerging as a potential synthesis protocol for various inorganic materials owing to its unique properties such as gas-like diffusivity, low viscosity and density [1, 2]. Recently, the supercritical fluids with these physico-chemical properties are explored in materials chemistry to design novel synthetic strategies for various materials [3, 4]. Various inorganic materials and composites have been synthesized at reduced temperature and time [5-8]. Graphene, a mono/few layer carbon sheet of graphite has attracted much attention in recent days due to their peculiar physico-chemical properties compared to graphite. However, the preparation and isolation of single layer (or) few layer graphene is still challenging issue. Hence, many synthetic strategies have been reported and attempts are in progress to prepare few layer graphene sheets [9-13]. Very recently, our group has reported supercritical fluid assisted synthesis of various inorganic materials, graphene exfoliation and chemical modification of graphene [14-16]. Recently, N-doped GNS materials have gathered much attention due to the possible amendment in electronic properties of graphene nanosheets. Thus, various attempts have been made to synthesis the N-doped GNS [17-37]. However, synthesis of N-doped GNS with desired amount of nitrogen and its site in the carbon network is still a challenging issue. Also, synthesis of large quantity of N-doped GNS with above feature is highly warranted towards commercial application. Here, we report the N-doped GNS synthesis via the supercritical fluid assisted method using graphene oxide and N-containing organic compounds as starting materials, and water and ethanol as solvent. And, the supercapacitor performance of N-doped GNS was examined in aqueous and ionic liquid electrolytes.

Experimental section

Supercritical fluid assisted preparation of N doped GNS

N-containing organic compounds, Ethylene diammine, melamine, hexa-methylene tetrammine and ethanol were used as received from Wako, Japan. GO solution (~35mg/mL) was prepared by modified Hummers method reported elsewhere [38, 39]. In a typical synthesis, N-containing organic compounds (Ethylenediamine or Melamine or hexamethylenetetramine) dissolved in ethanol solution was added into GO solution (~35 mg/mL), stirred for 30 min followed by ultrasonication for 30 min at room temperature. The ratio of GO and N-containing organic compound is maintained as 1:1 wt % for the all the experiments. Then, the above mixture was loaded into stainless steel reactors and the reactors were placed into pre-heated (400 °C) furnace with constant shaking (within a specifically

designed tubular furnace, AKICO, Japan). After 30 min, the reactors were quenched in an ice–water tank and the product was collected after several washings with distilled water and ethanol, and dried at 70 °C in a vacuum oven for 12 h (See supporting information for detailed synthesis processors). Since, the reactant solution contains water-ethanol mixture, the experiments were carried out at 400 °C and a pressure of 20 ~ 25 MPa (slightly above the supercritical temperature and pressure of water). After the supercritical treatment, the samples were reduced using hydrazine hydrate solution to ensure the reduction of GO nanosheets (See supporting information).

Materials Characterization

X-ray diffraction (XRD) patterns were collected on a RIGAKU (RINT2000 Tokyo, Japan) diffractometer using Ni-filtered Cu-K_α radiation (λ = 1.5418 Å). Thermogravimetry (TG) experiments (SII, TG/DTA 6300) were conducted in the temperature range of 25–800 °C in air using ~5-10 mg of the sample at the heating rate of 10 °C/min. The morphology of the nanocomposites was observed using a Hitachi-4800 field-emission scanning electron microscope (FE-SEM). Scanning and high-resolution transmission electron micrographs (STEM and HR-TEM) were recorded with a JEOL JEM-2100F microscope, working at an accelerating voltage of 200 kV. Fourier Transform Infrared (FT-IR) spectra were recorded in TENSOR 27 spectrometer (Bruker) using KBr pellet technique from 400 to 4000 cm^{-1}. The X-ray photoelectron spectra were recorded using a PHI5600, ESCA system with monochromated Al X-rays. Nitrogen adsorption and desorption isotherms were measured using Quantachrome Autosorb 1 sorption analyzer. All samples were outgassed for 2 h at 160 °C under vacuum in the degas port of the adsorption analyzer. The specific surface area was calculated using the BET model. The structure of the obtained nanocomposites was characterized using a micro-Raman system (HORIBA Scientific, Japan) equipped with a semiconducting laser with a wavelength of 532 nm.

Electrochemical Tests

The electrochemical performances of the prepared electrodes were characterized by cyclic voltammetry and galvanostatic charge-discharge measurements (Solartron 1260, USA) at different scan rates and current densities, respectively. The working electrodes were fabricated by mixing 85 wt% active material, 10 wt % conducting carbon black, and 5 wt % polytetrafluoroethylene (used as a binder, PTFE, Sigma Aldrich). The electrodes were dried

in a vacuum oven at 160 °C overnight before the electrochemical measurements. For cyclic voltammetry measurements, a conventional three electrode beaker type cell was used and the working electrode was fabricated by pressing the above paste on stainless steel mesh. Counter electrode was prepared by pressing the mixture of 80 wt % activated carbon (10 times higher than working electrode weight), 10 wt% aceyletene black and 10 wt% PTFE on stainless steel mesh. Ag/AgCl was used as reference electrode in aqueous electrolyte (1 M H_2SO_4). For voltammetry measurements in Ionic liquid medium, 1-ethyl-3-methylimidazoliumbis (trifluoromethane-sulfonyl) amide (EMI-TFSA) was used as electrolyte and silver wire in 0.01M Ag-TFSA/EMI-TFSA was used for the reference electrode. Galvanostatic charge-discharge measurements were carried out using two electrodes system at various current densities. The specific capacitance of the electrode materials was calculated from the galvanostatic discharge process according to the following equation [17] $C_{single} = 4 \times I \times \Delta t / (\Delta V \times m)$. Where, I is the discharge current (A), Δt is the discharge time (s), ΔV is the voltage change during the discharge process (excluding the IR drop), and m is the total mass of the active material in both side of the electrodes (g). The samples synthesized from supercritical reaction with GO and N-containing organic compounds such as ethylenediamine, melamine and hexamethylenetetramine are described as NE-GNE, NM-GNS and NH-GNS, respectively, in subsequent discussions.

Results and discussion

Figure 1 shows the FE-SEM images of N-doped GNS obtained from the supercritical fluid assisted reaction of N-containing organic compounds and GO. The transparent and loosly packed nature of the N-doped GNS indicates the formation of few layered N-doped GNS during the supercritical process. Also, it can be clearly seen from the images that the physical structure nature of the N-doped graphene nanosheets are does not affected by the supercritical fluid treatment. At high magnification (Fig 1b), the assembly of graphene nanosheets could be seen clearly, that enables the electrolyte to permeate through the electrode materials and access all the available electrode surface for the electrochemical charge storage. Only sheets like morphology is observed throughout the N-doped graphene samples that clearly indicates the decomposition of N-containing organic compounds during the supercritical treatment does not leave any other carbonaceous impurities such as nanospheres, nanocables, nanofibers, and submicrotubes. To ensure that there is no adsorbed N-containing organic compounds on the graphene sheets, TG analysis were performed from

room temperature to 800 °C in air. TG profile of all there N-doped samples shows (Fig S1) almost a similar decomposition pattern. The insignificant weight loss up to 400 °C indicates the absence of physisorbed and chemisorbed N-containing organic compounds on N-doped GNS. At above 400 °C, the decomposition of N-doped GNS starts and complete decomposition was observed at 620 °C, there was no residue after 620 °C indicating the absence of any other impurities in the N-doped GNS. BET surface area analysis were carried out to estimate the specific surface area of N-doped GNS, it shows a specific surface area of 230 m^2/g, 182 m^2/g and 216 m^2/g for NE-GNS, NM-GNS and NH-GNS, respectively.

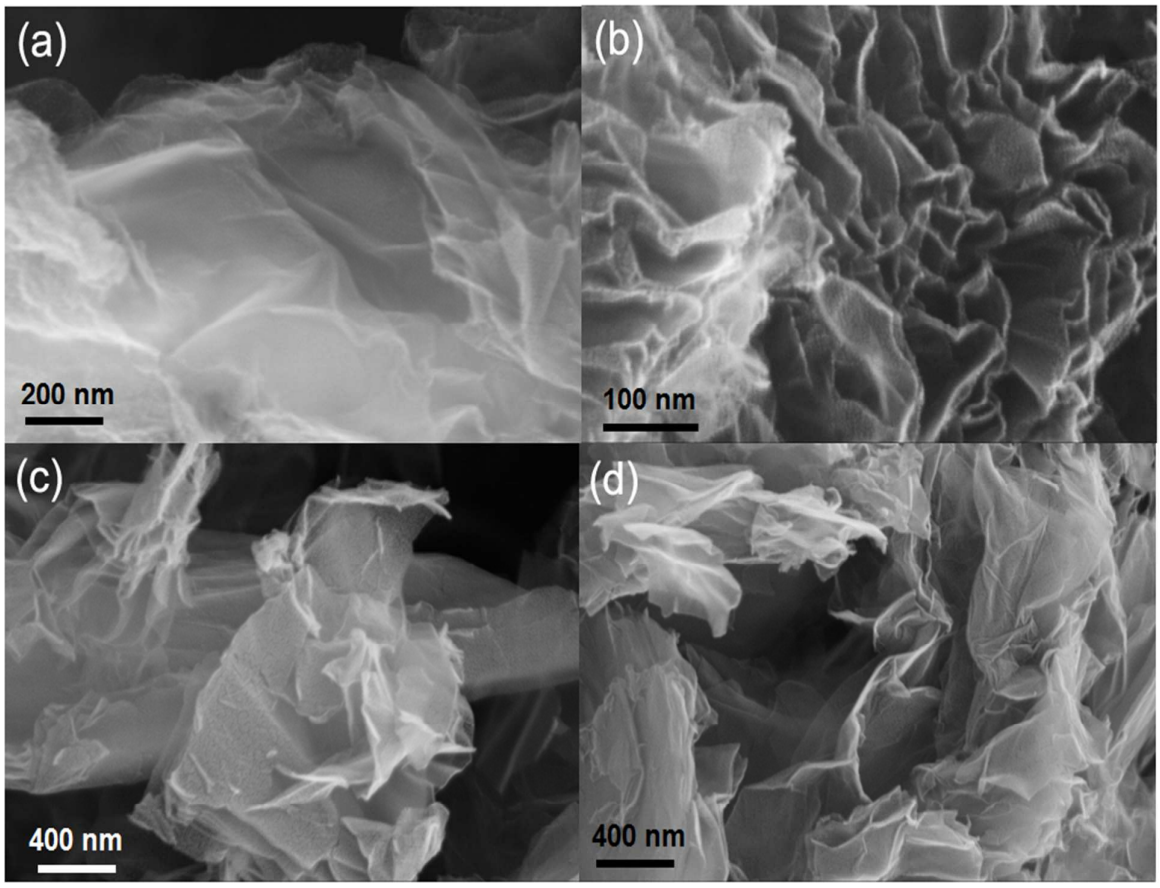

Fig. 1 FE-SEM images of (a & b) NE-GNS, (c) NM-GNS and (d) NH-GNS.

Figure 2 shows the representative TEM images of GO nanosheets and N-doped GNS prepared by the supercritical fluid assisted synthesis. N-doped GNS exhibit very similar appearance like GO sheets, it clearly indicates that the fluid treatment does not affect the

physical structure of the GNS significantly. Indeed, a few layers of N-doped GNS formation could be clearly seen from the highly transparent GNS.

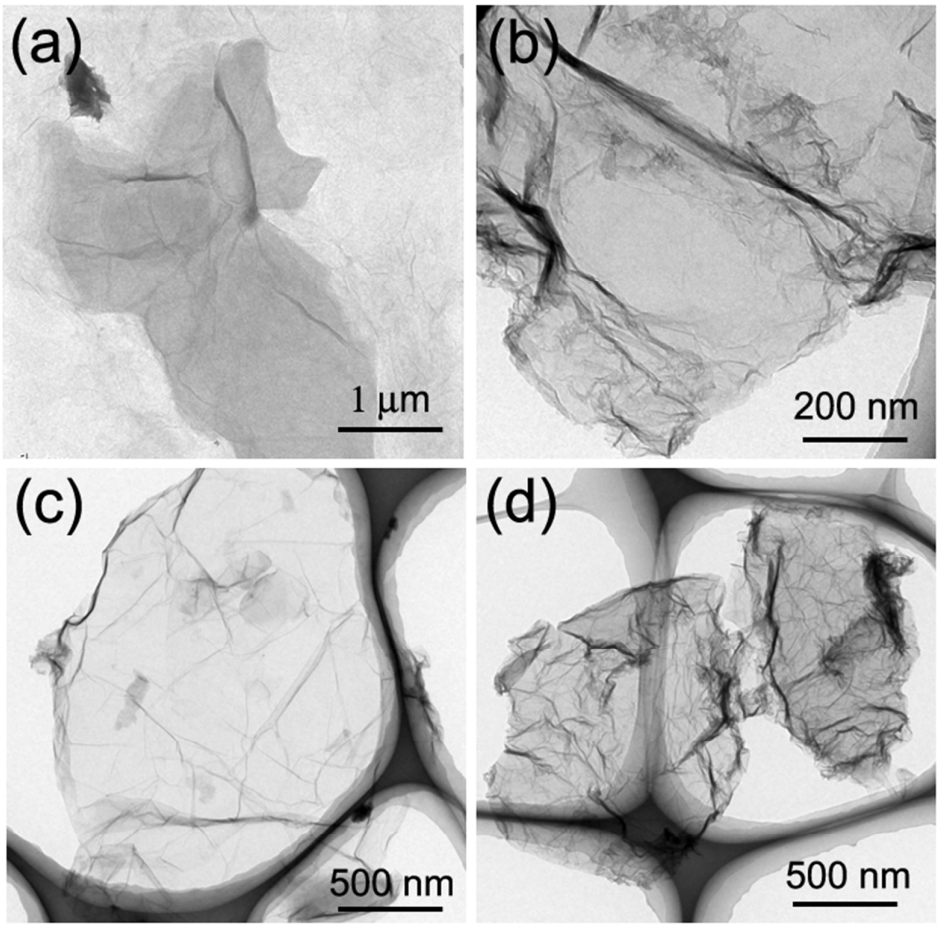

Fig. 2 TEM images of (a) as-prepared GO nanosheets, (b) NE-GNS, (c) NM-GNS and (d) NH-GNS.

To understand the chemical nature of the prepared N-doped GNS, Raman spectroscopic characterization was carried out. Raman spectroscopy is a powerful analytical tool to distinguish different kind of bonding nature in carbon materials [40-42]. It has been widely accepted that, it can preciously distinguish sp^2 and sp^3 hybridized bonding of carbon atoms in GNS and extensively used to estimate graphene layer thickness [42-44]. The G band and the D band intensity are assigned to the E_{2g} phonon of sp^2 carbon atoms and the extent of defects in the graphene, respectively [42-45]. In Figure 3, the intensity of the D band (I_D) at 1336 cm^{-1} of NE-GNS and NM-GNS are almost equal to the G band intensities (I_G) or slightly lower than G band, that is the I_D/I_G ratio is less than 1, indicating the low level defect

structure. Whereas, the I_D/I_G ratio of NH-GNS is higher than 1, indicating the more defects in the graphene structure due to the strong oxidation during the supercritical fluid treatment. In addition, the G band position is slightly shifted to lower frequency than the other two N-doped GNS. It is reported that the shift in G band towards lower frequency is proportional to graphene layer thickness. The slight shift observed for the NH-GNS might be the indication of few layers GNS than other two samples. FT-IR spectrum of GO and N-doped graphene nanosheets are compared in Fig S2. For GO nanosheets, the observed peaks at 1726 cm^{-1}, 1616 cm^{-1}, 1251 cm^{-1}, 1081 cm^{-1} and 800 cm^{-1} are assignable to C=O stretching of COOH, aromatic C=C groups, C-O stretching of epoxy, C-O stretching of alkoxy and C=C bending in GO nanosheets, respectively [46]. For N-doped graphene nonosheets, the O-containing functional groups such as C=O stretching of COOH, C-O stretching of epoxy and C-O stretching of alkoxy peaks are drastically reduced/completely disappeared. And, few additional vibration peaks corresponding to C=N stretching and C-N stretching in benzenenoid ring are observed at 1555 cm^{-1} and 1204 cm^{-1}, for the N-doped graphene nanosheets, respectively [46, 47]. NM-GNS shows two additional peaks at 1515 cm^{-1} and 1345 cm^{-1} corresponding to N-O stretching. The NE-GNS shows a strong peak corresponding to presence of C-O stretching of alkoxy groups at 1068 cm^{-1}, however the peak corresponding to C-O stretching of epoxy groups at 1251 is completely disappeared. It clearly indicates that the decomposition of N-containing organic compounds during the supercritical treatment introduces N-doping in the GNS and the nature of N-doping in the GNS various with nature of the N-containing compounds.

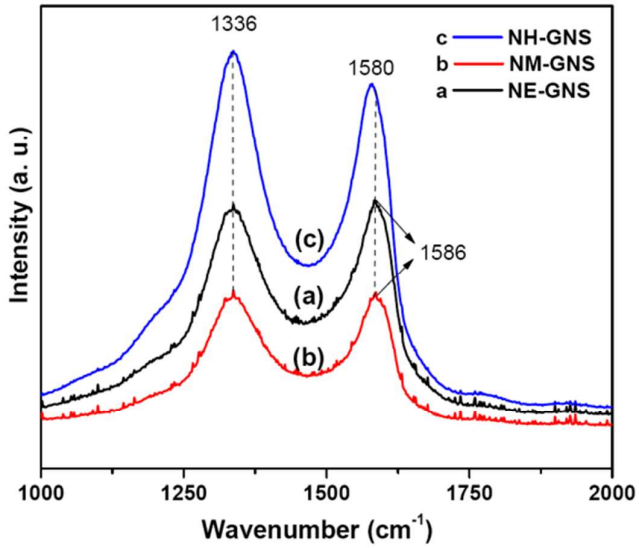

Fig 3. Raman spectra of (a) NE-GNS, (b) NM-GNS and (c) NH-GNS

XPS is a powerful and highly reliable tool to identify the elements' states and its concentration in the sample by analysis of binding energy (BE) values and the peak intensity, respectively. The XPS spectra of N-doped GNS samples are shown in Figure 4. The XPS survey spectra of N-doped GNS shows three distinguished peaks at 284.6, 399.6 and 532.3 eV corresponding to C1s of sp2 C, N1s of the doped N, and O1s, respectively [24]. The intensity of the N1s peak varies with nature of the starting materials used for the N-doped GNS. The XPS survey spectra of RGO prepared using supercritical fluid treatment was shown in Fig S3. The O1s peak looks similar in all the three N-doped GNS samples indicating the existence of certain amount of unreduced or oxygen containing functional groups on N-doped GNS surface. The broad XRD line observed at $2\theta=10°$ for the N-doped GNS strongly supports to the above conclusion.

To understand the binding nature of the N in the GNS, the C1s and N1s binding energy value were investigated in detail. On deconvolution, the high resolution C1s peak can be fitted into four peaks at 284.5, 285.9, 288 and 289 eV [S4-S6, supporting information]. The sharp peak at 284.5 eV with 74% intensity was attributed to the sp2 carbon atoms in the N-doped GNS [26]. The other small peaks observed at 285.9 and 288 ascribed to the existence of different N-sp^2C, N-sp^3C originating from the substitutional doping of N atom in GNS [27-30]. Another small peak observed at 289 eV was ascribed to the C-O bonding configurations in the N-doped GNS [30, 32], indicates the existence of unreduced oxygen containing functional groups on the N-doped GNS. Similarly, the deconvolution of high resolution N1s peak [Figure 4d-f] indicates the presence of three peaks at 398.5, 399.8 and 401.2 corresponding to the presence of pyridinic N, pyrrolic N and quaternary N in the N-doped GNS, respectively [26,28-32, 33, 35]. The above observed binding energy values are in good correspondence with the literature reported values [37]. Thus, the supercritical fluid assisted syntheses of N-doped GNS by reacting GO and N-containing organic compounds successfully introduce N-atoms in the graphene backbone. The amount of N-atom doping (atomic %) is estimated using XPS for the N-doped GNS obtained different N-containing organic compounds and it is estimated that 4.71, 2.02 and 5.31% for NE-GNS, NM-GNS and NH-GNS, respectively. It could be clearly seen that the order of N-doping in GNS is NH-GNS > NE-GNS > NM-GNS. Similarly, the CHN analysis also shows same order of N-doping in the N-doped GNS samples.

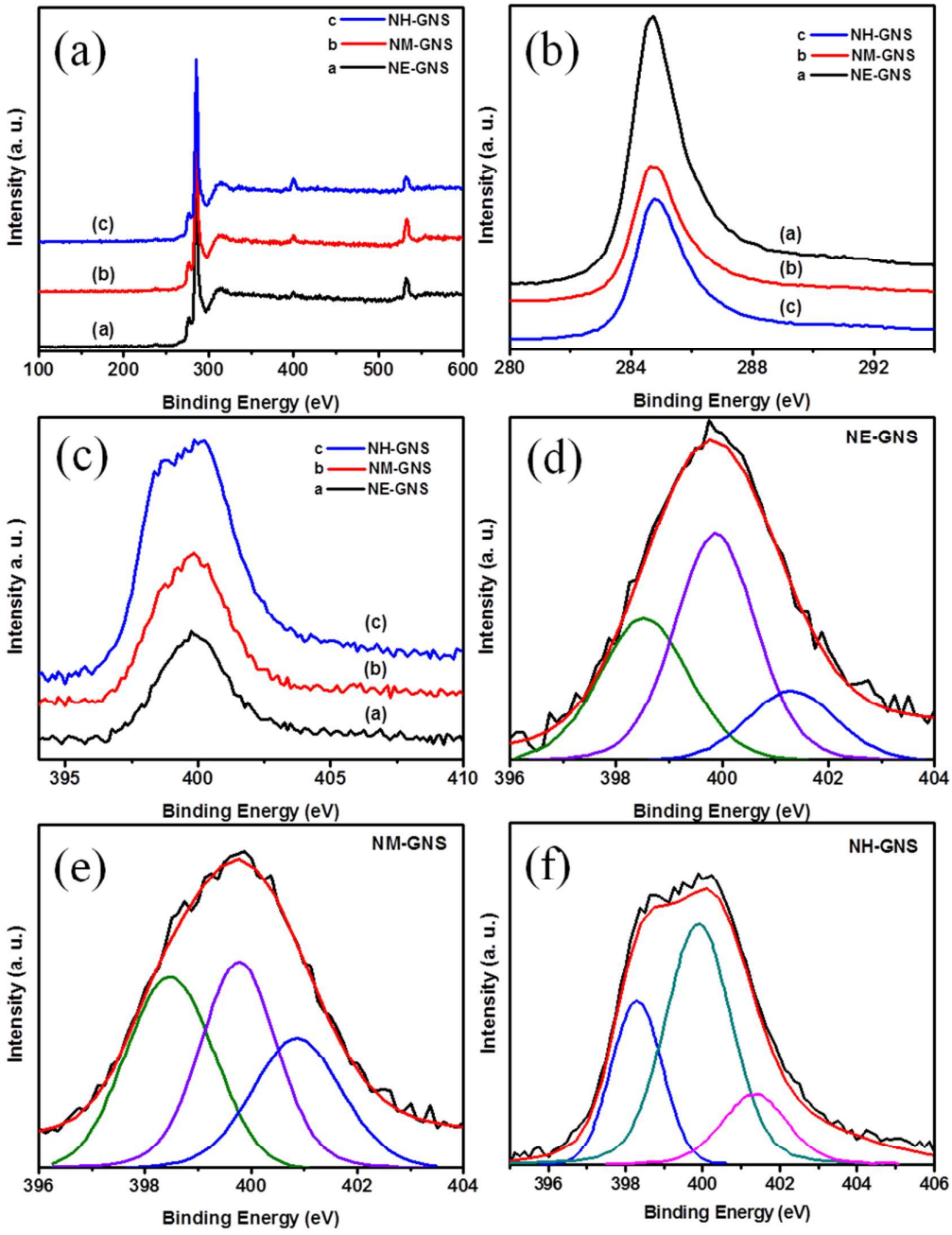

Fig.4. XPS spectra of (a) N-doped GNS, (b) N1s, (c) O1s, (d) N1s of NE-GNS, (e) N1s of NM-GNS and (f) N1s of NH-GNS

Figure 5 shows the XRD pattern of N-doped GNS and RGO nanosheets prepared in supercritical fluid treatment and GO nanosheets. The XRD pattern of the N-doped GNS shows a broad peak at 13.6° corresponding to (002) plane of GO and a sharp peaks at 25.6° and 43.8° corresponding to graphite like structure [28, 29]. The XRD line corresponding to

the GO (002) plane is shifted to slightly higher 2θ values compared to pristine GO. This indicates that the functional group on the GO surface was reduced or removed significantly by N-containing organic compounds during the N-doping process at supercritical condition [48, 49]. Besides, the observed 2θ values for graphite like structure are slightly lower than pristine graphite. It hints that the graphene sheets in the N-doped GNS are stacked weakly due to the N-doping or the presence of N-containing functional groups on N-GNS. Among the all the three samples, NH-GNS shows strong line corresponding to GO and weak line corresponding to graphite. NM-GNS shows relatively higher graphitic nature than other two samples.

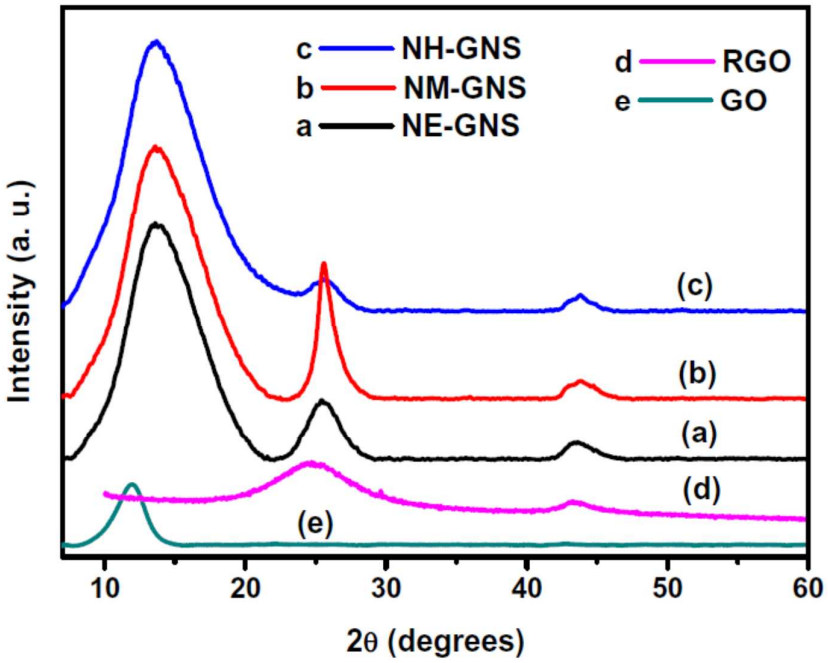

Fig 5. X-ray diffraction patterns of (a) NE-GNS, (b) NM-GNS, (c) NH-GNS, (d) RGO and (e) GO nanosheets

To evaluate the potential of the N-doped GNS as an electrode in supercapacitors, the EDLC behaviour was measured in aqueous and ionic liquid electrolyte. Figure 6a shows the cyclic voltammetry curves of N-doped GNS in 1M H_2SO_4 electrolyte at 10 mV/s scan rate. It could be clearly seen that the N-doped GNS shows pure EDLC behaviour in the studied potential range. Figure 6b shows the galvanostatic charge-discharge profile of the N-doped samples in 1M H_2SO_4 electrolyte at 0.5A current rate. Among the three N-doped samples, NE-GNS shows a specific capacity of 280 F/g. And, NM-GNs and NH-GNS show a specific capacity of 176F/g and 132F/g, respectively. For comparison purpose, pure GNS was also

prepared using the similar supercritical fluid assisted treatment (without N-doping) and it shows a specific capacitance of 127 F/g (Fig S7). It clearly indicates that the N-doping on GNS has significant influence in the specific capacitance. The observed specific capacitance (both in aqueous and ionic electrolytes) for the N-doped GNS is in good correspondence with their specific surface area of 230 m^2/g (NE-GNS), 182 m^2/g (NM-GNS) and 216 m^2/g (NH-GNS). Though, the order of specific surface area and specific capacitance of N-doped samples are same in this case, the change in specific capacitances with specific surface area is highly asymmetrical. Thus, it is believed that the amount of N-doping and chemical nature has major role on the specific capacitance. The electrode stability was measured for 100 cycles for the N doped GNS electrodes, the results shows that there is no significant change in the specific capacitance during the charge-discharge (Figure 8a). The NH-GNS shows a very slight increase in the specific capacity whereas the other two electrodes a slight decrease in specific capacity with charge-discharge cycling.

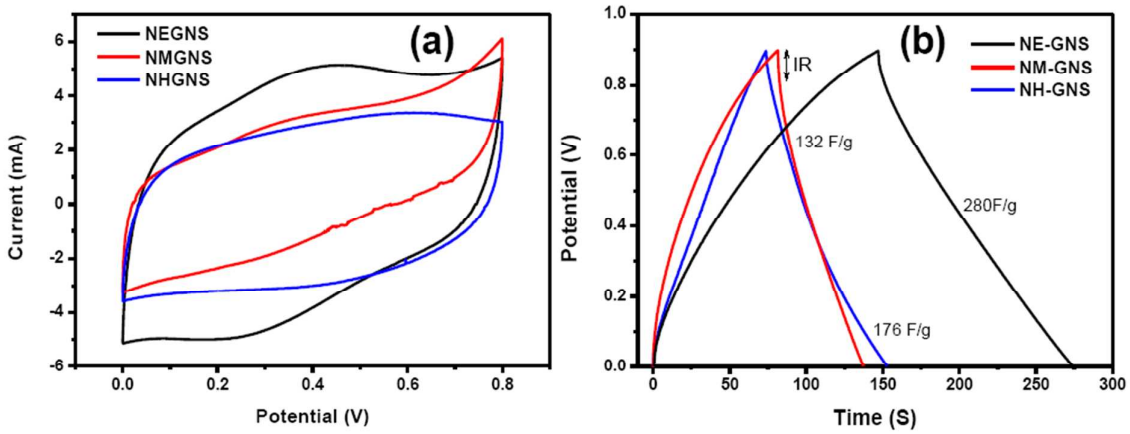

Fig 6. CV profiles of N-doped GNS (a) and charge-discharge profile of N-doped GNS in 1M H_2SO_4 electrolyte

The electrochemical performance of the N-doped GNS was evaluated using ionic liquid (EMI-TFSA) as electrolyte. The CV studies were performed between -2.25 to +0.2.0 V, a 4.25V potential window and the corresponding profile are shown in Figure 7a. Figure 7b shows the galvanostatic charge-discharge profile of the N-doped samples from 0 to 3.6 V in EMI-TFSA electrolyte at 0.05A current rate and the specific capacitance was calculated using the equation 1. NE-GNS shows higher specific capacitance of 104 F/g which is much higher than the NH-GNS (56 F/g) and NM-GNS (25F/g). Though, the CV shows a stable profile at 4.25V in three electrode system, the galvanostatic charge-discharge measurement was unable

to carry out up to 4.25 V in two electrode system. Even in 3.6 V charge-discharge profile, it could be clearly seen that a large IR drop was observed in the ionic liquid. It may be ascribed to high internal resistance due to the poor conductivity and high viscosity of the ionic liquids compared to aqueous electrolytes [50] that results higher resistance between the electrode and electrolyte interface. The electrode stability was measured for 100 cycles for the NE-GNS electrode and the observed results shows that there is a drastic decrease in the specific capacitance up to 35 then it increase slightly and become stable at 40~50 F/g for 100 cycles. (Figure 8b)

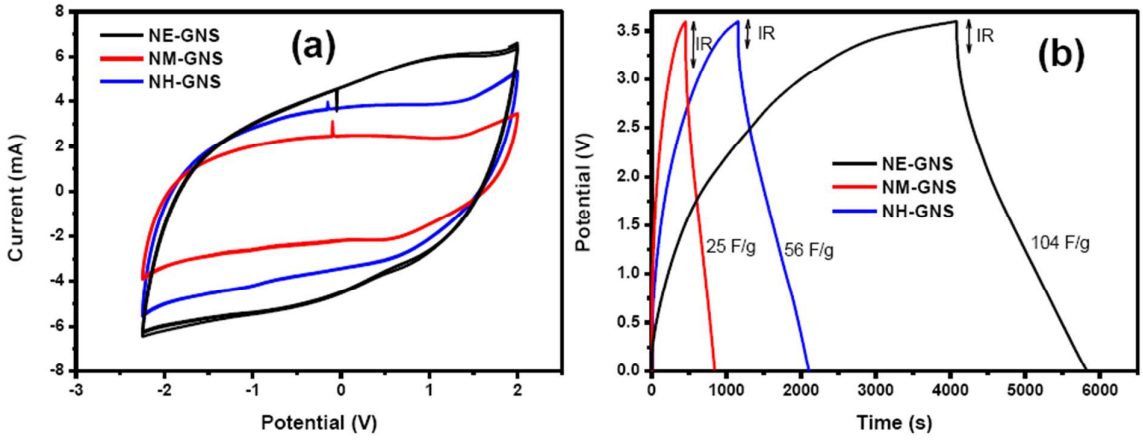

Fig 7. CV profiles of N-doped GNS (a) and charge-discharge profile of N-doped GNS in EMI-TFSA electrolyte

NE-GNS electrode shows an energy density of 8 Wh/Kg and 40 Wh/Kg in 1M H_2SO_4 and EMI-TFSA, respectively. However, the energy density observed in the ionic liquid medium is not stable as the capacitance values are decreasing with cycling. Certainly, an energy density of 16 Wh/Kg was retained after 100 cycles of charge-discharge. Optimization of various parameters such as N-content, electrolyte, quality of graphene sheets etc may improve the electrode performance and stability in the ionic electrolyte medium. Thus, it is believed that N-doped GNS are promising electrode materials for high energy supercapacitors applications.

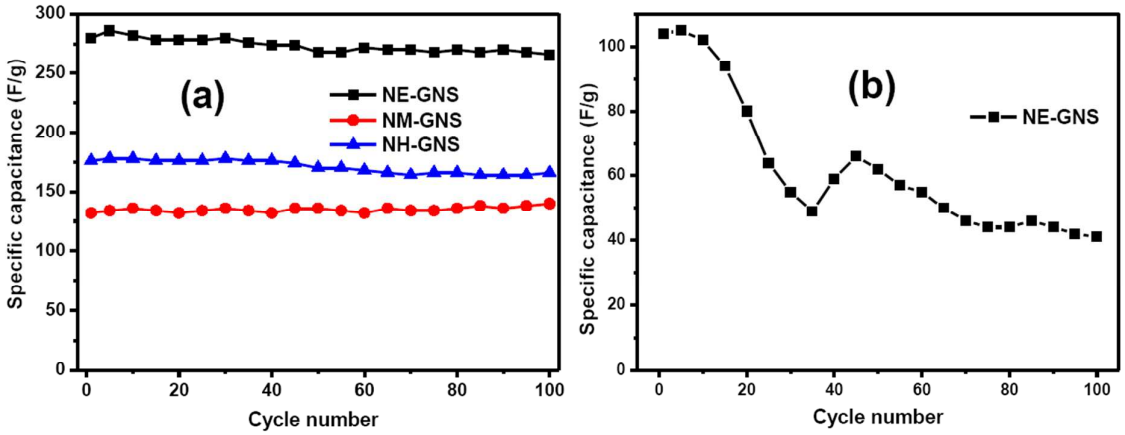

Fig 8. Cycle performance of (a) N-doped GNS in 1M H_2SO_4 electrolyte at 1A/g current rate (b) NE-GNS electrode in EMI-TFSA electrolyte at 0.05A/g current rate

Conclusions

Supercritical fluid assisted reaction of N-containing organic compounds with GO solution results the formation of N-doped GNS. The amount of N-doping depends on the nature of N-containing organic compound. XPS reveals the presence of pyridinic N, pyrrolic N and quaternary N in the N-doped GNS samples. The amount of N-doping varies with nature of the N-containing organic compounds. FE-SEM and TEM images show the presence of loosely packed few layer N-doped GNS. And Raman spectroscopic characterization confirms the presence of few layer N-doped GNS. FT-IR spectroscopic analysis revealed the presence of various N-containing functional groups on N-doped GNS surface. XRD diffraction analysis reveals the weakly stacked N-doped GNS due to the N-doping or the presence of N-containing functional groups on N-doped GNS. Among, the N-doped GNS, NE-GNS show a high specific capacitance of 280 F/g and 104 F/g in aqueous 1M H_2SO_4 and inionic liquid EMI-TFSA, respectively. It shows an energy density of 8 Wh/Kg and 40 Wh/Kg in 1M H_2SO_4 and EMI-TFSA, respectively. The cyclic voltammetry and charge-discharge studies show the capacitance behaviour and stability of N-doped GNS electrodes in aqueous and ionic liquids. The supercapacitance performance of the N-doped GNS samples depends on the amount of N-doping as well as nature of N-doping in the graphene.

References

1. G. K. Serhatkulu, C. Dilek and E. Gulari, *J. Supercrit. Fluids*, 2006, **39**, 264.
2. K. P. Johnston and P. S. Shah, *Science*, 2004, **303**, 482.
3. T. Adschiri, Y. Hakuta and K. Arai, *Ind. Eng. Chem. Res*., 2000, **39**, 4901
4. T. Adschiri, K. Kanazawa and K. Arai, *J. Am. Ceram. Soc*., 1992, **75**, 2615.
5. R. Sui and P. Charpentier**,** *Chem. Rev.*, 2012, **112**, 3057.
6. C. Aymonier, A. Loppinet-Serani, H. Reveron, Y. Garrabos and F. Cansell, *J. Supercrit. Fluids,* 2006, **38**, 242.
7. M. Bahrami and S. Ranjbarian, *J. Supercrit. Fluids*, 2007, **40**, 263.
8. W. Qian, X. Cui, R. Hao, Y. Hou and Z. Zhang, *ACS Appl. Mater. Interfaces*, 2011, **3**, 2259.
9. A. Balandin, S. Ghosh, W. Z. Bao, I. Calizo, D. Teweldebrhan, F. Miao and C. N. Lau, *Nano Lett*., 2008, **8**, 902.
10. K. S. Novoselov, A. K. Geim, S. V. Morozov, D. Jiang, M. I. Katsnelson, I. V. Grigorieva, S. V. Dubonos and A. A. Firsov, *Nature*, 2005, **438**, 197.
11. K. S. Novoselov, Z. Jiang, Y. Zhang, S. V. Morozov, H. L. Stormer, U. Zeitler, J. C. Maan, G. S. Boebinger, P. Kim and A. K. Geim, *Science*, 2007, **315**, 1379.
12. D. A. Dikin, S. Stankovich, E. J. Zimney, R. D. Piner, G. H. B. Dommett, G. Evmenenko, S. T. Nguyen and R. S. Ruoff, *Nature*, 2007, **448**, 457.
13. C. Lee, X. D. Wei, J. W. Kysar and J. Hone, *Science*, 2008, **321**, 385.
14. D. Rangappa, K. Sone, M. Wang, U. K. Gautam, D. Golberg, H. Itoh, M. Ichihara and I. Honma, *Chem. Eur. J*., 2010, **16**, 6488.
15. J. H. Jang, D. Rangappa, Y. U. Kwon and I. Honma, *J. Mater. Chem*., 2011, **21**, 3462.
16. D. Rangappaa, M. Ichihara, T. Kudo and I. Honma, *J. Power Sources*, 2009, **194**, 1036.
17. L. L. Zhang, X. Zhao, H. Ji, M. D. Stoller, L. Lai, S. Murali, S. Mcdonnell, B. Cleveger, R. M. Wallace and R. S. Ruoff, *Energy Environ. Sci.,* 2012, **5**, 9618.
18. D. Geng, Y. Chen, Y. Chen, Y. Li, R. Li, X. Sun, S. Ye and S. Knights, *Energy Environ. Sci.,* 2011, **4**, 760.
19. Y. Q. Zhang, D. K. Ma, Y. Zhuang, X. Zhang, W. Chen, L. L. Hong, Q. X. Yan, K. Yu and S. M. Huang, *J. Mater. Chem*., 2012, **22**, 16714.

20. S. Wang, L. Zhang, Z. Xia, A. Roy, D. W. Chang, J. B. Baek and L. Dai, *Angew. Chem. Int. Ed*., 2012, **51**, 4209.

21. L. Qu, Y. Liu, J. B Baek and L. Dai, *ACS Nano*, 2010, **4**, 1321

22. Y. Li, Y. Zhao, H. Cheng, Y. Hu, G. Shi, L. Dai, and L. Qu, *J. Am. Chem. Soc*., 2012, **134**, 15.

23. C. Zhang, R. Hao, H. Liao and Y. Hou, Nano Energy, 2013, **2**, 88.

24. Y. Wang, Y. Shao, D. Matson, J. Li and Y. Lin, *Acs Nano*, 2010, **4**, 1790.

25. H. L. Guo, P. Su, X. Kang and S. K. Ning, *J. Mater. Chem. A*, 2013, **1**, 2248.

26. D. Wei, Y. Liu, Y. Wang, H. Zhang, L. Huang and G. Yu, *Nano lett.,* 2009, **9**, 1752.

27. Z. Luo, S. Lim, Z. Tian, J. Shang, L. Lai, B. MacDonald, C. Fu, Z. Shen, T. Yu and J. Lin, *J. Mater. Chem*., 2011, **21**, 8038.

28. S. Van Dommele, A. Romero-Izquirdo, R. Brydson, K. P. de Jong and J. H. Bitter, *Carbon*, 2008, **46**, 138.

29. D. C. Wei , Y. Q. Liu , Y. Wang , H. L. Zhang , L. P. Huang and G. Yu, *Nano Lett*., 2009, **9**, 1752.

30. C. Zhang, L. Fu, N. Liu, M. Liu, Y. Wang and Z. Liu, *Adv. Mater.,* 2011, **23**, 1020.

31. E. Yoo, J. Nakamura and H. Zhou, *Energy Environ. Sci.,* 2012, **5**, 6928.

32. D. Marton, K. J. Boyd, A. H. Al-Bayati, S. S. Todorov and J. W. Rabalais, *Phys. Rev. Lett*., 1994, **73**, 118.

33. J. R. Pels, F. Kapteijn, J. A. Moulijn, Q. Zhu and K. M. Thomas, *Carbon*, 1995, **33**, 1641.

34. Y. Mao, H. Duan, B. Xu, L. Zhang, Y. Hu, C. Zhao, Z. Wang, L. Chen and Y. Yang, *Energy Environ. Sci.,* 2012, **5**, 7950.

35. D. Deng, X. Pan, L. Yu, Y. Cui, Y. Jiang, J. Qi, W.-X. Li, Q. Fu, X. Ma, Q. Xue, G. Sun and X. Bao, *Chem. Mater*., 2011, **23**, 1188.

36. Z. Li, Z. Xu, X. Tan, H. Wang, C. M. B. Holt, T. Stephenson, B. C. Olsen and D. Mitlin, *Energy Environ. Sci.,* 2013, **6**, 871.

37. Y. Shao, S. Zhang, M. H. Engelhard, G. Li, G. Shao, Y. Wang, J. Liu, I. A. Aksay and Y. Lin, *J. Mater. Chem*., 2010, **20**, 7491.

38. W. S. Hummers and R. E. Offeman, *J. Am. Chem. Soc*., 1958, **80**, 1339.

39. L. J. Cote, F. Kim and J. Huang, *J. Am. Chem. Soc*., 2009, **131**, 1043.

40. L. M. Malard, M. A. Pimenta, G, Dresselhaus and M. S. Dresselhaus, *Phys. Rep*., 2009, **473**, 51.

41. A. C. Ferrari, J. C. Meyer, V. Scardaci, C. Casiraghi, M. Lazzeri, F. Mauri, S. Piscanec, D. Jiang, K. S. Novoselov, S. Roth and A. K. Geim, *Phys. Rev. Lett*., 2006, **97**,187401.

42. B. Das, R. Voggu, C. S. Rout and C. N. R. Rao, *Chem. Commun*., 2008, 5155.

43. F. Tuinstra and J. L. Koenig, *J. Chem. Phys*., 1970, **53**, 1126.

44. D. B. Shinde, J. Debgupta, A. Kushwaha, M. Aslam and V. K. Pillai, *J. Am. Chem. Soc*., 2011, **133**, 4168.

45. C. Zhang, N. Mahmood , H. Yin , F. Liu and Y. Hou, *Adv. Mater*. **2013**, 25, 4932.

46. T. N. Huan, T. V. Khai, Y. Kang, K. B. Shim and H. Chung, *J. Mater. Chem.***,** 2012, **22**, 14756.

47. Z. D. Zujovic and J. B. Metson, *Langmuir*, 2011, **27**, 7776.

48. D. C. Marcano, D. V. Kosynkin, J. M. Berlin, A. Sinitskii, Z. Sun, A. Slesarev, L. B. Alemany, W. Lu and J. M. Tour, *ACS Nano*, 2010, **4**, 4806.

49. Y. Qian, A. Vu, W. Smyrl and A. Steina, *J. Electrochem. Soc., 2012,* **159,** A1135

50. T. Y. Kim, H. W. Lee, M. Stoller, D. R. Dreyer, C.W. Bielawski, R. S. Ruoff, and K. S. Suh, *ACS Nano*, 2011, **5**, 436.

Graphical abstract:-

Supercritical Fluid Assisted Synthesis of N-doped Graphene Nanosheets and Its Capacitance Behavior in Ionic liquid and Aqueous Electrolyte

M. Sathish, S. Mitani, T. Tomai, and I. Honma**

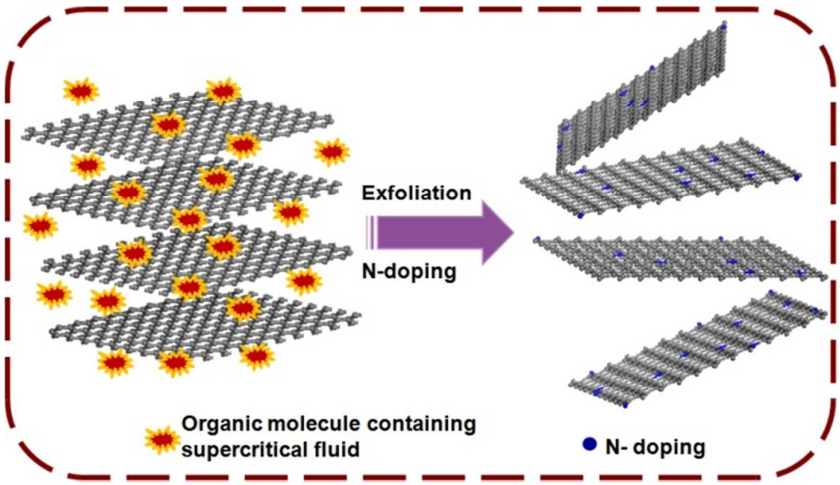

N-doped GNS have been prepared using single step supercritical fluid assisted reaction of N-containing organic compounds with graphene oxide (GO) solution. It shows a specific capacitance of 280 F/g in aqueous 1M H_2SO_4 (0.8 V) and 104 F/g in ionic liquid EMI-TFSA (3.6V) with an energy density of 8 Wh/Kg and 40 Wh/Kg, respectively.